Synthesis of ZSM-23 (MTT) zeolites with different crystal morphology and intergrowths: effects on the catalytic performance in the conversion of methanol to hydrocarbons

A. Molino,[a] J. Holzinger,[b] K. A. Łukaszuk,[a] D. Rojo-Gama,[a] A. E. Gunnæs,[c] J. Skibsted,[b] L. F. Lundegaard,[d] S. Svelle,[a] P. Beato,[d] S. Bordiga[a,e] and K. P. Lillerud[a]

[a.] *Center for Materials Science and Nanotechnology, Department of Chemistry, University of Oslo, Oslo, Norway*
[b.] *Interdisciplinary Nanoscience Center (iNANO), and Department of Chemistry, Aarhus University, Denmark*
[c.] *Department of Physics, University of Oslo, Oslo, Norway*
[d.] *Haldor Topsøe A/S, Lyngby, Denmark*
[e.] *Department of Chemistry, NIS and INSTM Reference Centre, University of Torino, Via G. Quarello 15, 10135 Torino, Italy*

Supplementary Information

1. Refined XRD data (Figures S 1-5)
2. Description of the MTT and TON topology (Figures S 6-7)
3. Simulations of powder XRD pattern of MTT/TON faulted structures (Figure S 8)
4. Residual electron density (Figures S 9-11)
5. Atomic coordinates of the refined MTT structure (Table S 1)
6. Crystal length distribution (Figure S 12)
7. FTIR spectra of ZSM-23 samples in presence of CO - region around 2000 cm^{-1} (Figure S 13)
8. ^{29}Si MAS NMR and ^{29}Si $\{^{1}H\}$ CP/MAS NMR spectra (Figure S 14)
9. Nitrogen adsorption/desorption curves (Figure S 15)

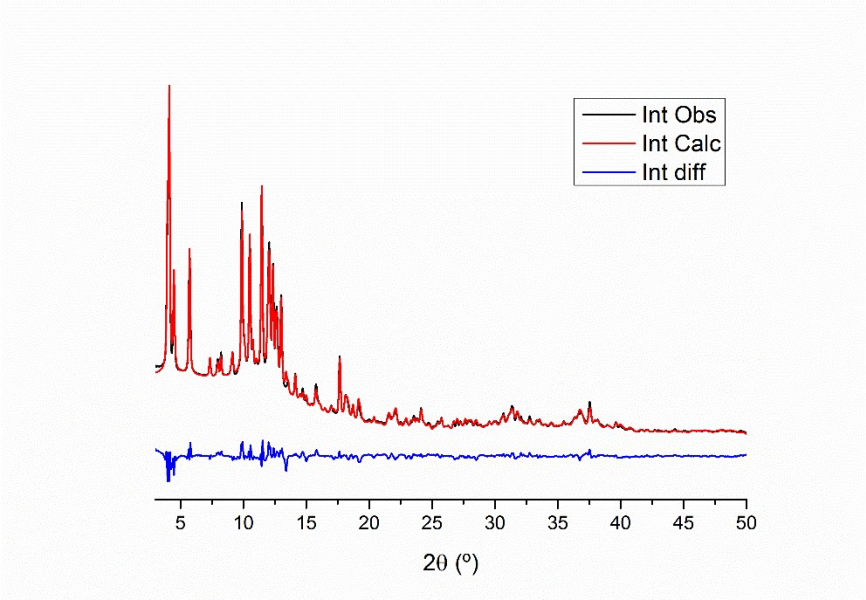

Figure S 1. Rietveld refinement of DIQUAT ZSM-23 zeolite using the model with $Pmn2_1$ symmetry.

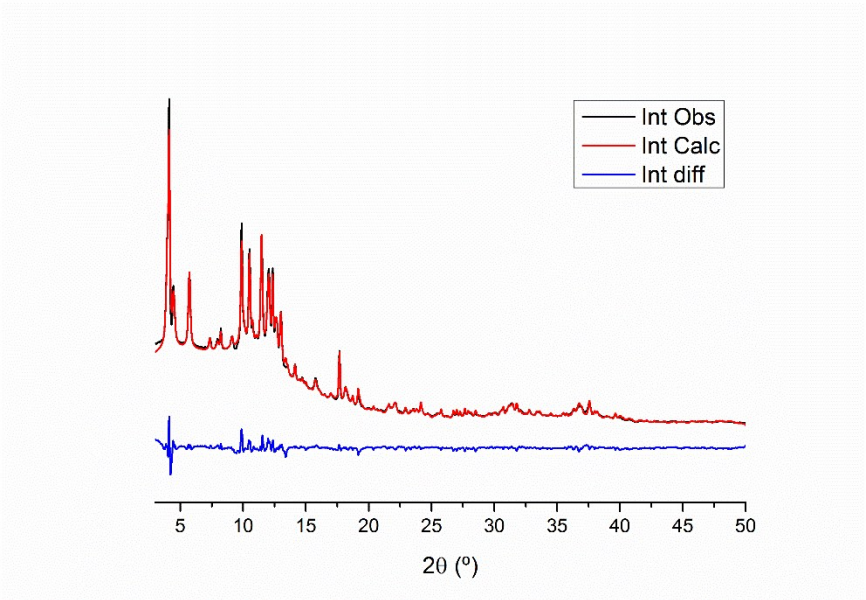

Figure S 2. Rietveld refinement of PYRR ZSM-23 zeolite using the model with $Pmn2_1$ symmetry.

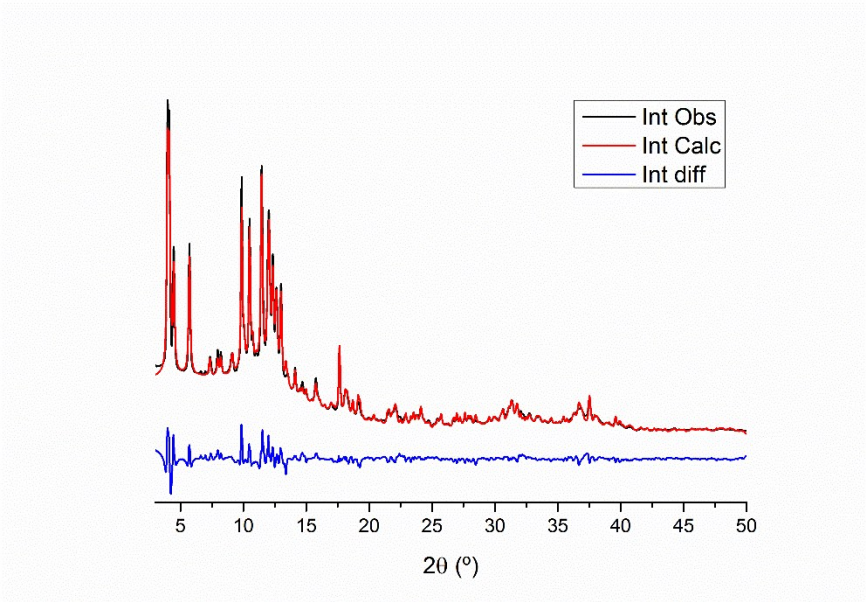

Figure S 3. Rietveld refinement of HTMPD ZSM-23 zeolite using the model with $Pmn2_1$ symmetry.

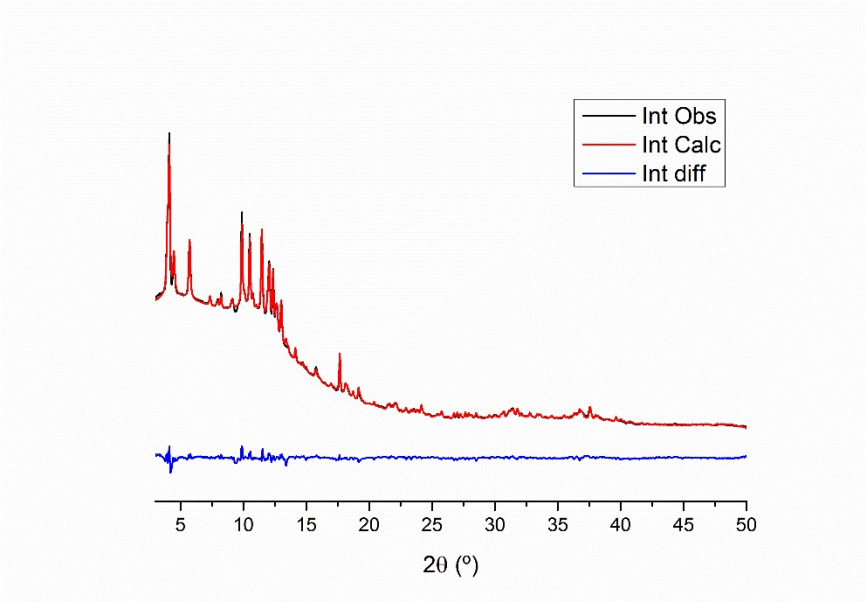

Figure S 4. Rietveld refinement of IPA ZSM-23 zeolite using the model with $Pmn2_1$ symmetry.

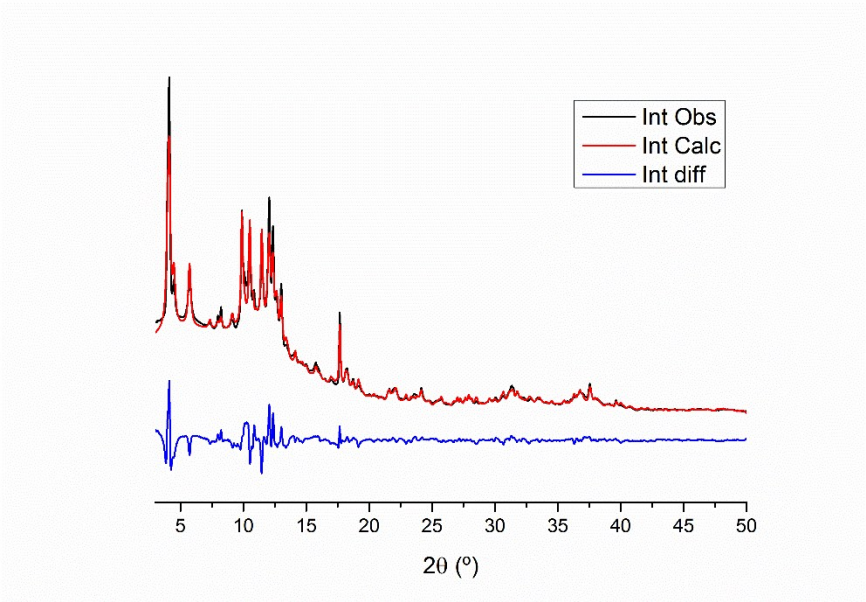

Figure S 5. Rietveld refinement of DMF ZSM-23 zeolite using the model with $Pmn2_1$ symmetry.

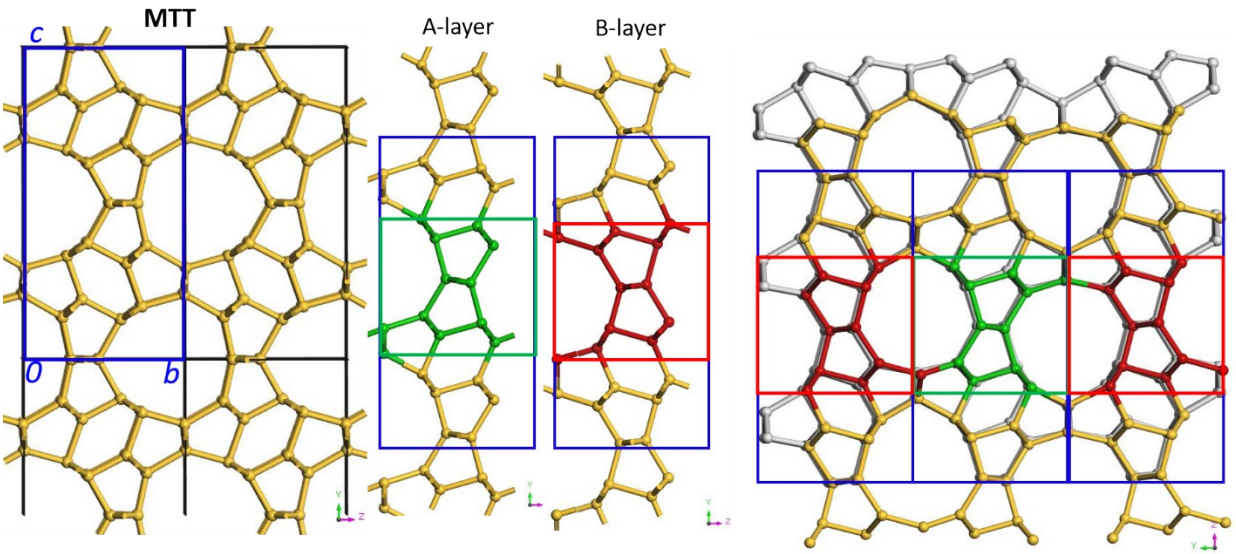

Figure S 6. The MTT (ZSM-23) structure can be generated by stacking alternating A-layers (indicated in green) and B-layers (indicated in red, atomic coordinates are given in the DIFFaX input file). To generate the MTT structure a -0.56 shift in the a-direction is needed, this is orthogonal to the drawing and not visible. In the right panel, A-layers and B-layers are stacked on top of the regular MTT structure given in grey.

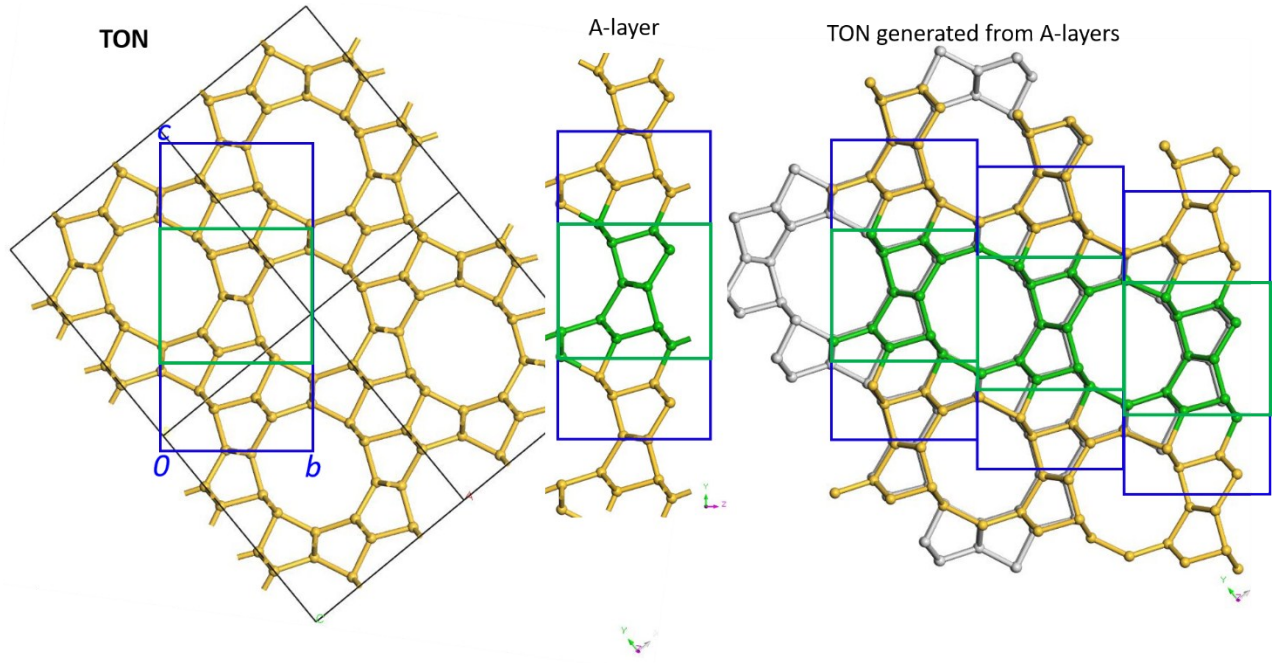

Figure S 7. The TON (ZSM-22) structure can be generated by stacking the A-layer (unit indicated in green, atomic coordinates are given in the DIFFaX input file). This "unit-cell" is half the size of the regular MTT-unit-cell (indicated in blue). To generate the TON structure, a -0.22 shift in the c-direction is needed.

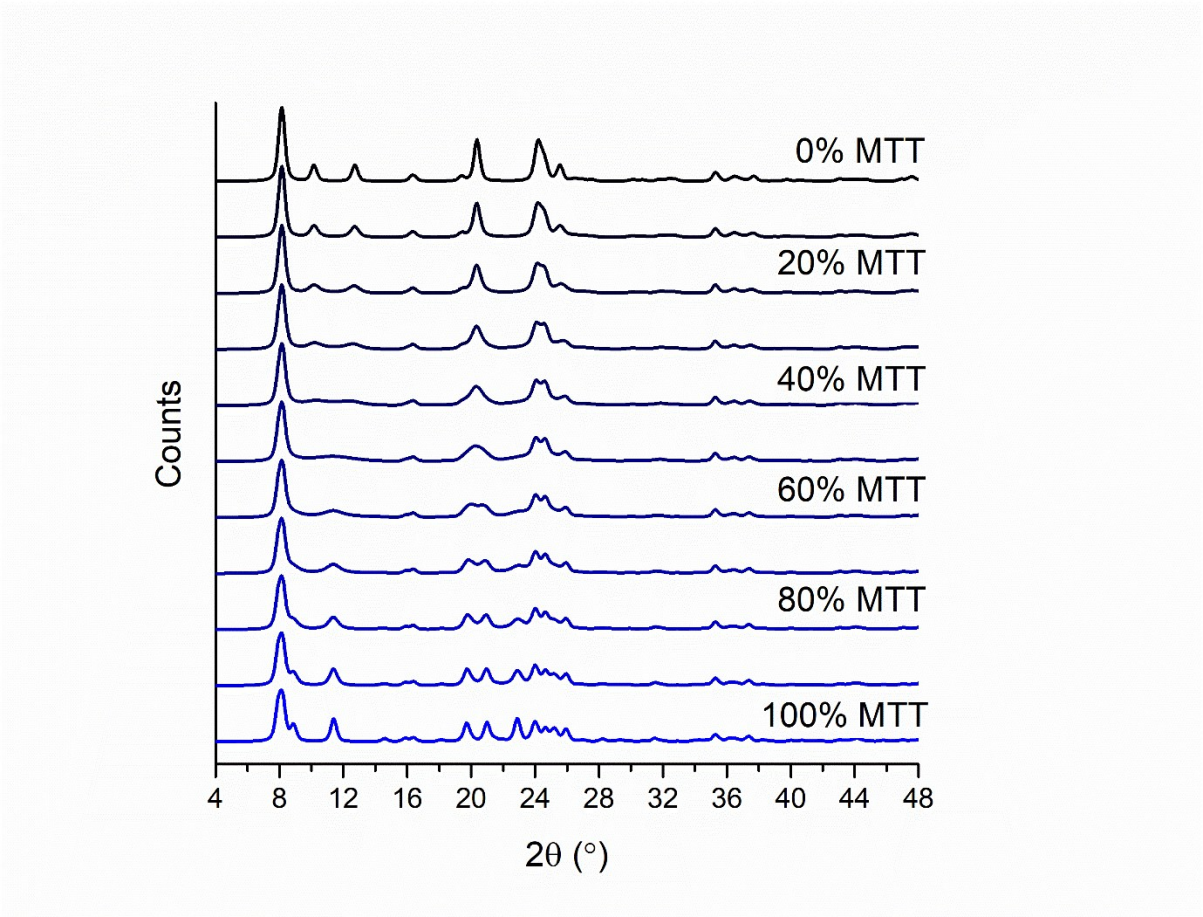

Figure S 8. Simulation of powder XRD patterns (λ = 1.5406 Å) using DIFFaX of MTT/TON random intergrowths with different probabilities of faulting (shown in increments of 10%). Top: pure TON structure, bottom: pure MTT structure.

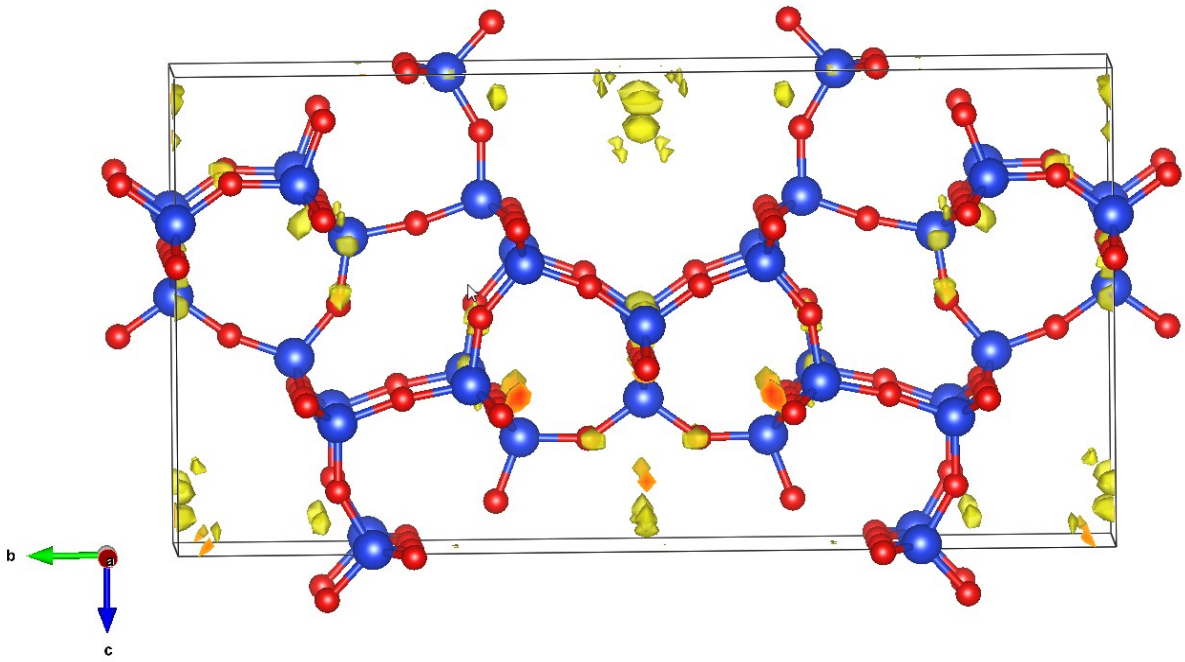

Figure S 9. Plot showing the residual electron density (in yellow) of the DIQUAT sample after refinement with the ZSM-23 structure with Pmmn symmetry.

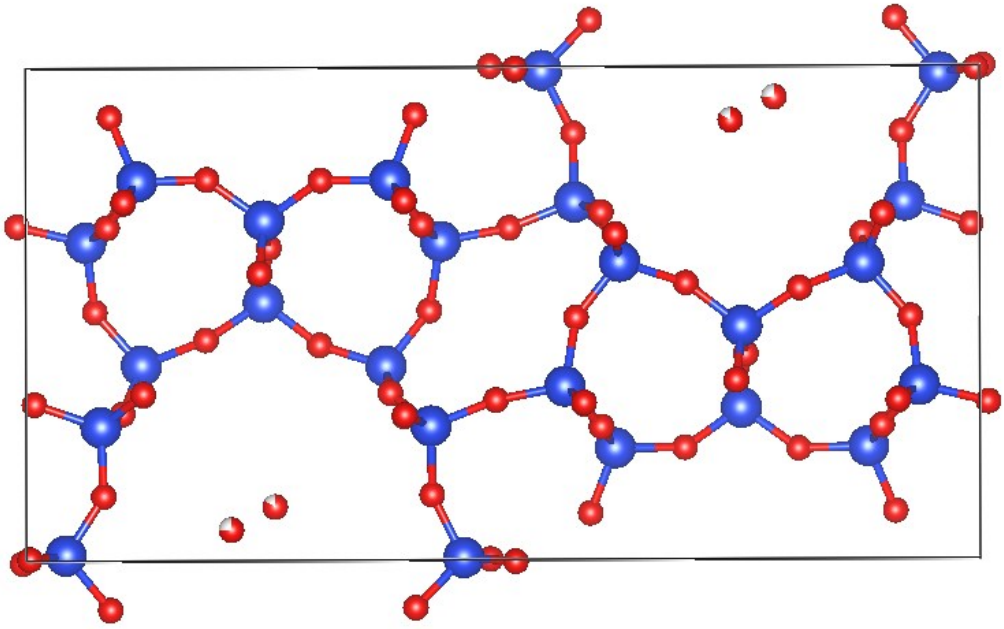

Figure S 10. Plot showing the residual electron density (in yellow) of the DIQUAT sample after refinement with the ZSM-23 structure with $P2_1$ symmetry.

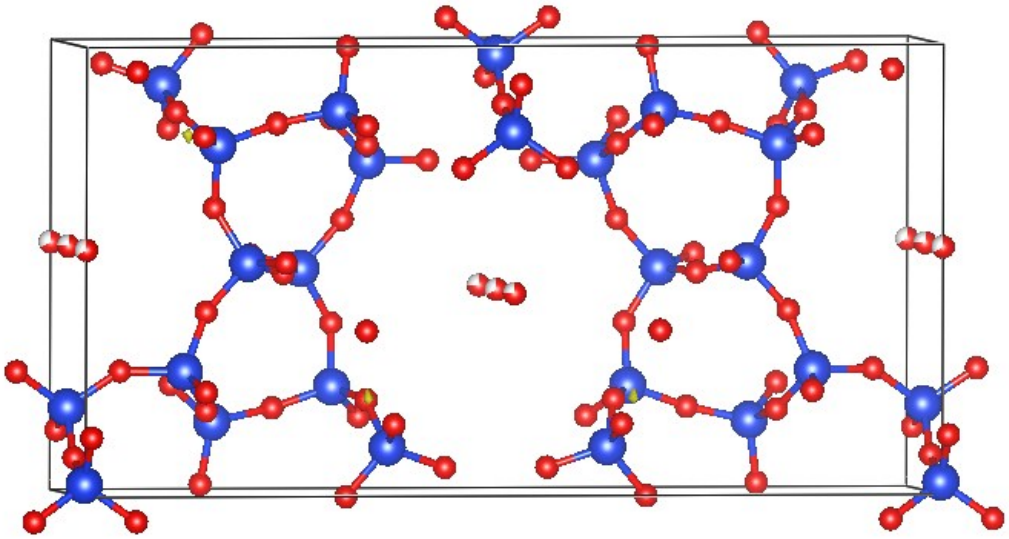

Figure S 11. Plot showing the residual electron density (in yellow) of the DIQUAT sample after refinement with the ZSM-23 structure with $Pmn2_1$ symmetry.

Table S 1. Atomic coordinates of the refined MTT structure with $Pmn2_1$ symmetry.

Atom	**X**	**Y**	**Z**	**Occupancy**
Si(1)	0.3722(5)	0.101(1)	0.52(1)	1
Si(2)	0.1331(5)	-0.727(1)	0.55(1)	1
Si(3)	0.1730(5)	-0.2243(11)	0.53(1)	1
Si(4)	0.3135(5)	-0.1497(13)	0.55(1)	1
Si(5)	0	-0.8091(16)	0.46(1)	1
Si(6)	0.2084(5)	-0.4914(12)	0.47(1)	1
Si(7)	0.5	-0.0262(15)	0.46(1)	1
O(1)	0.0603(8)	-0.728(2)	0.50(1)	1
O(2)	0.1734(9)	-0.365(2)	0.47(1)	1
O(3)	0.3262(9)	-0.010(2)	0.499(13)	1
O(4)	0.441(1)	0.056(2)	0.488(14)	1
O(5)	0.2415(9)	-0.174(2)	0.514(14)	1
O(6)	0.1585(9)	-0.5949(19)	0.507(11)	1
O(7)	0.1449(13)	-0.201(2)	0.818(11)	1
O(8)	0.1316(11)	-0.157(3)	0.318(12)	1
O(10)	0.5	-0.133(3)	0.673(13)	1
O(12)	0.148(1)	-0.771(2)	0.843(11)	1
O(14)	0.1666(12)	-0.816(2)	0.344(1)	1
O(13)	0.2593(13)	-0.499(3)	0.70(1)	1
O(15)	0	-0.915(3)	0.673(13)	1
O(a)	0.5	0.45	0	0.64(3)
O(b)	0.5	0.45	0.5	0.64(3)

a)

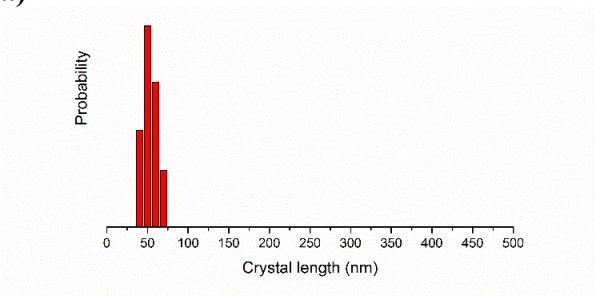

b)

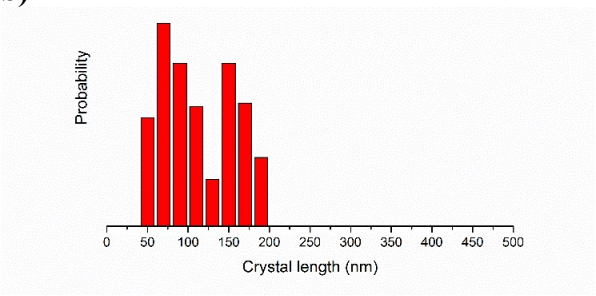

c)

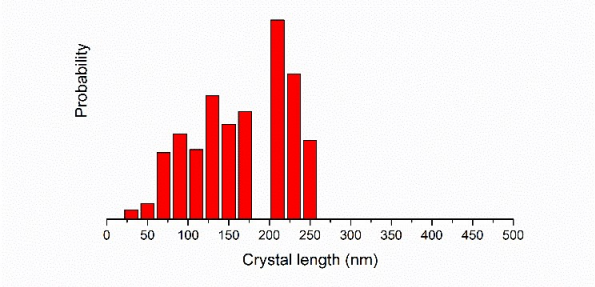

d)

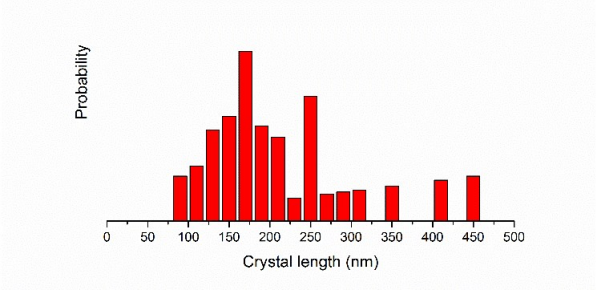

e)

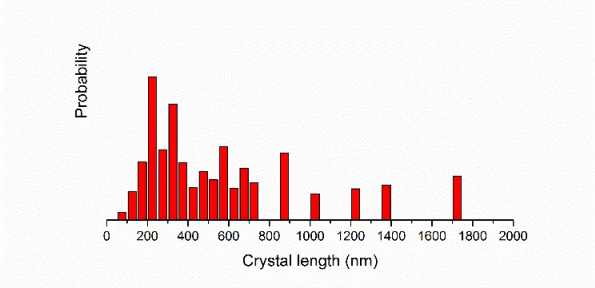

Figure S 12 Distribution (in mass) of crystal length of different ZSM-23 samples: a) DIQUAT, b)PYRR, c) IPA, d) HTMPD, e) DMF.

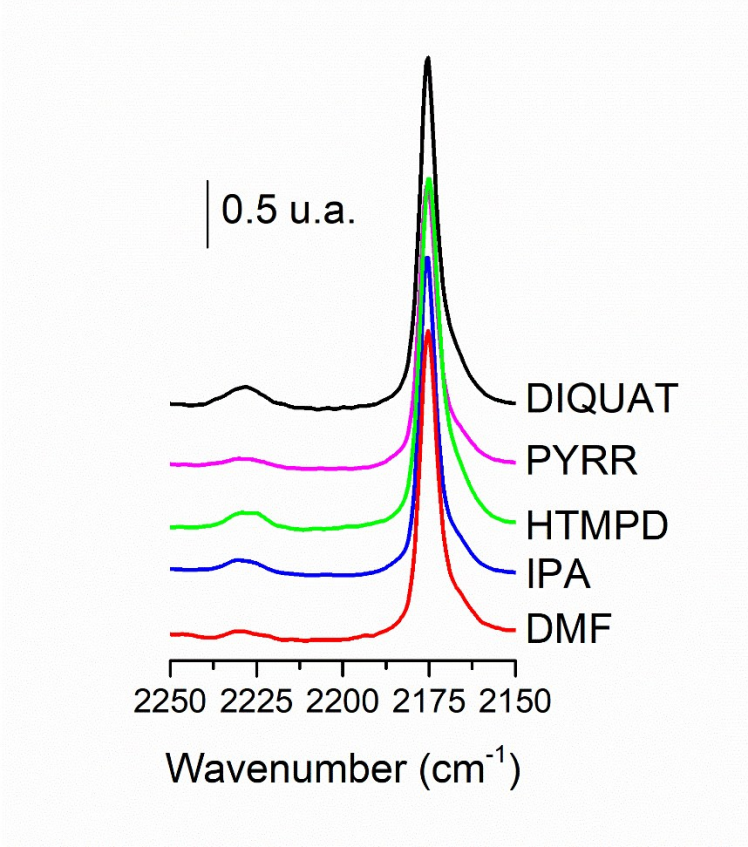

Figure S 13. Region around 2000 cm^{-1} of the FTIR spectra of ZSM-23 samples in presence of CO at equilibration pressure of 0.065 mbar. The spectra are shifted for clarity.

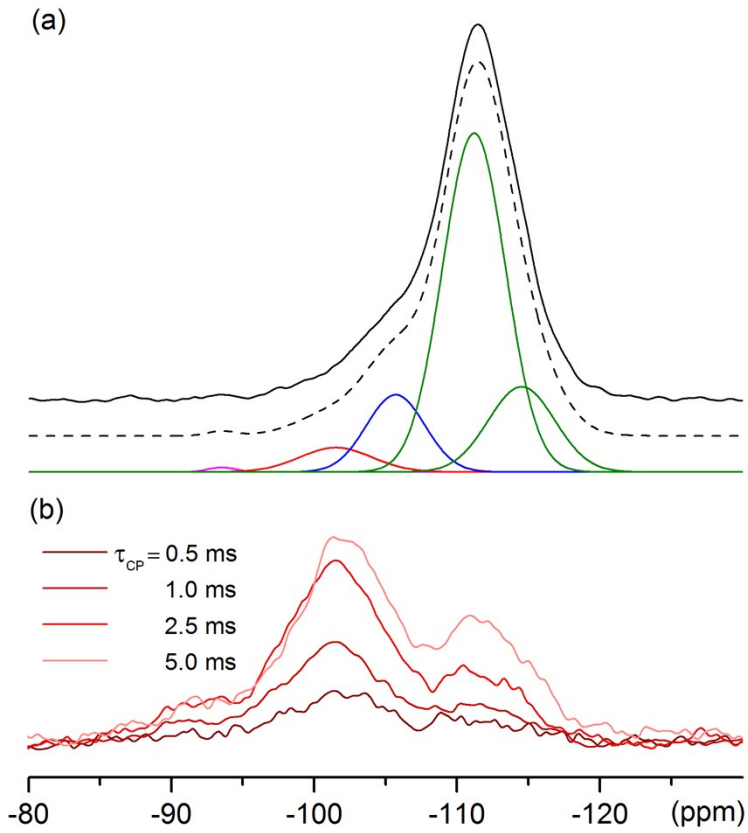

Figure S 14. (a) Single-pulse ^{29}Si MAS NMR spectrum (B_0 = 7.05 T, ν_R = 7.0 kHz) for the H-ZSM-23 sample DIQUAT including its deconvolution (Q^2{0Al} magenta; Q^3{0Al} red; Q^4{1Al} blue; Q^4{0Al} green). (b) The corresponding ^{29}Si {^{1}H} CP/MAS NMR spectra (B_0 = 9.4 T, ν_R = 7.0 kHz) obtained with CP contact times of 0.5 – 5.0 ms.

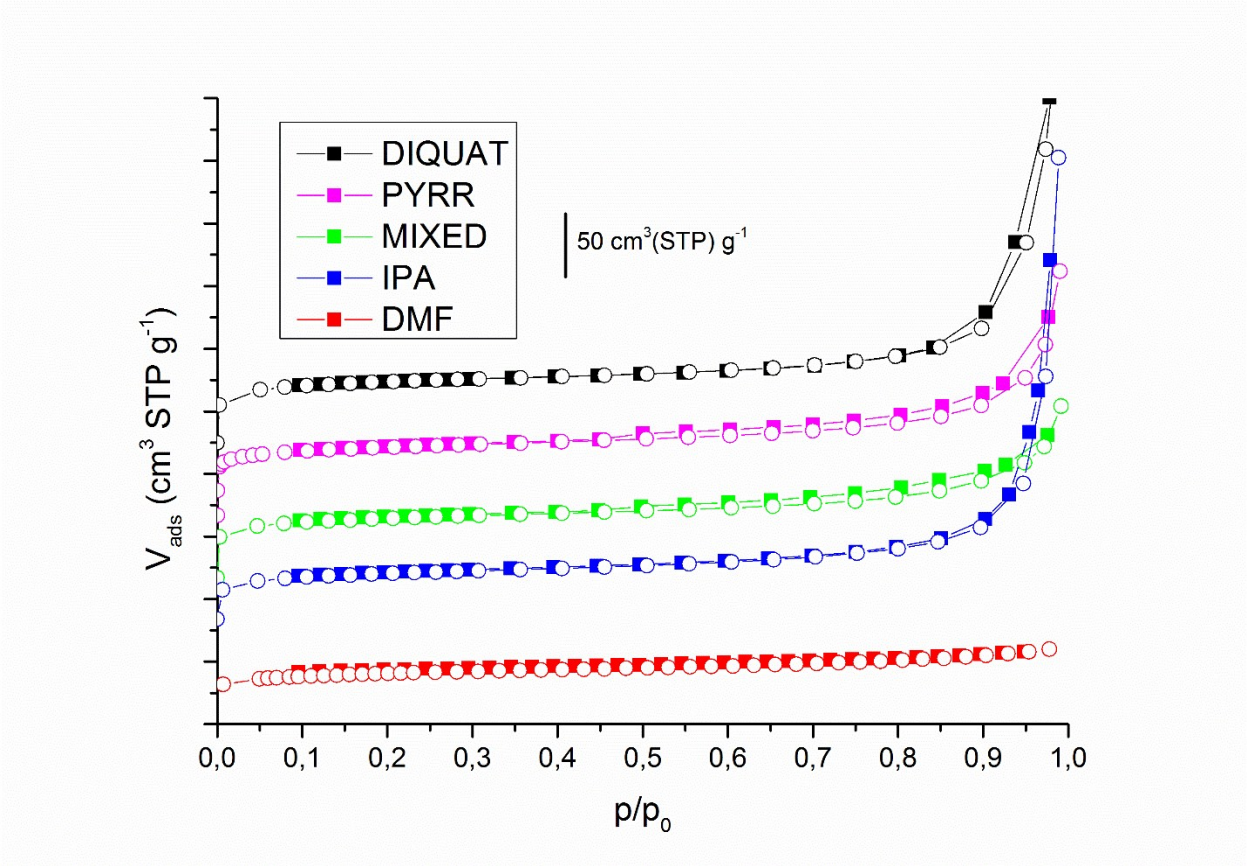

Figure S 15. Nitrogen adsorption (circles) and desorption (squares) for the H-ZSM-23 samples. The graphs are shifted for clarity.